This is the peer reviewed version of the following article: [Accelerated Development of High Voltage Li-Ion Cathodes. Advanced Energy Materials 12, 40 p2201704 (2022)], which has been published in final form at https://doi.org/10.1002/aenm.202201704.

Accelerated development of high voltage Li-ion cathodes

Antranik Jonderian[1, †], Shipeng Jia[1,†], Gabin Yoon[2], Victor Teodor Cozea[1], Nooshin Zeinali Galabi[1], Sang Bok Ma[2,*] and Eric McCalla[1,*]

[1] Department of Chemistry, McGill University, Montreal, Canada

[2] Battery Material Lab, Samsung Advanced Institute of Technology, Samsung Electronics, Suwon, Gyeonggi-do 16678, Republic of Korea

[†] Contributed equally.

* Corresponding authors: eric.mccalla@mcgill.ca and sangbok.ma@samsung.com

Abstract:

High voltage cathodes are attractive for high energy density Li-ion batteries. However, candidates such as $LiCoPO_4$ have presented numerous challenges stemming from poor electronic/ionic conductivities such that typical solutions involving nanosizing result in extremely poor cycling performance. Here, we apply high-throughput methods to develop near-micron sized carbon-coated $LiCoPO_4$ with improved energy density and capacity retention. In total, 1300 materials with 46 different substituents were synthesized and characterized. A number of substituents showed greatly improved capacity (e.g. 160 mAh/g for 1% In substitution vs. 95 mAh/g for the pristine). However, co-doping was required to improve extended cycling. $Li_{1-3x}Co_{1-2x}In_xMo_xPO_4$ was found to be particularly effective with dramatically improved cycling (as high as 100 % after 10 cycles, vs. ~50 % in unsubstituted). While In improved the electronic conductivity of the carbon-coated materials, Mo co-doping gave larger particles and DFT calculations showed that Mo impedes the formation of Li/Co antisite defects.

Summary:

The performance of a high-voltage Li-ion cathode, $LiCoPO_4$, is systematically improved through high-throughput experimentation wherein doping and co-doping is performed on the Co site. Low-level doping of indium (1 %) and a second dopant (Mo, Nb in particular) show the best performance for both energy density and extended cycling. The reasons for the improvements are explored with DFT and experiments.

1. Introduction

There is a global demand for higher energy storage devices for electric vehicles in order to improve their range and become attractive for widespread use. One of the primary approaches to increasing energy density is to use cathodes that operate at higher voltages. $LiCoPO_4$ (LCP) has garnered a great deal of attention in this regard, as it operates near 4.8 V *vs*. Li.[1] To date, liquid electrolytes have not been able to operate at such high potentials although significant progress is being made.[2] Furthermore, the promise of stable solid electrolytes also serves to renew our interest in LCP. However, the challenges are numerous, with the key problems being that LCP is an electronic and ionic insulator. The only commercialized cathode with such poor intrinsic transport properties is $LiFePO_4$ (LFP) for which the limitations are overcome by nanosizing and carbon-coating the particles such that the poor transport takes place over very short length scales.[3] In the case of LFP, the greatly increased surface area due to nano-sizing is not detrimental given that the cathode operates at 3.45 V where liquid electrolytes are perfectly stable.[3] By contrast, LCP operates outside of the stability window of typical electrolytes such that nanosizing may indeed improve the first cycle capacity (e.g. capacities ranging from 80 mAh/g for 1-2 micron sized particles up to 125 mAh/g for 100-200 nm particles), but it is disastrous for extended cycling.[4] Typically, in the undoped materials, when the first cycle capacities of the approach 130 mAh/g due to nanosizing, the capacity retention is very poor (e.g. approximately 25% retention after 10 cycles in ref. [5]). As there is also a dramatic range of results in the literature for the impact of dopants in this material[1,6–18], there is a need for a systematic study where synthesis and test conditions are uniform to truly determine the impact of all the potential dopants. Previous computational work[6] demonstrated that a number of dopants are expected to be possible and interestingly all those explored lowered the

redox voltage compared to the undoped. Herein, we report the first systematic study of 46 different dopants (shown in the periodic table in Figure S1) and co-dopants into micron sized LCP.

2. Results and discussion

As described in the methods section, a sol-gel synthesis is used wherein uncoated LCP is first made in air at either 750 or 850 °C. The resulting LCP materials are then mixed with a carbon source before being heated under forming gas to make carbon-coated LCP. Figure 1a shows the typical workflow followed here wherein wide substitutions are explored using high-throughput methods, followed by characterization/DFT on key compositions prior to proposing/performing further high-throughput on co-doped samples. Figure 1b shows that the undoped material is pure phase LCP, while the cyclic voltammogram (CV) performed in high-throughput between 3.0 and 5.3 V at 0.2 V/h is also shown in Figure 1. The results for undoped LCP yield a first discharge capacity of 95 mAh/g at 850 °C, and 104 mAh/g at 750 °C, consistent with undoped materials with micron sized particles (shown in the SEM image in Figure 2) as per ref.[4]. The capacity retention after 10 cycles are only 47 % (850 °C) and 43 % (750 °C). The slightly improved capacity and diminished retention at the lower synthesis temperature are attributed to smaller particles. It is important to recognize that a CV up to 5.3 V is a cycling protocol that leads to extremely poor extended cycling (i.e. all samples will spend 3 h above 5.0 V on every cycle, this is in contrast to galvanostatic cycling where LCP materials spend no time above 5.0 V). This cycling protocol is therefore ideal to rapidly obtain discrimination (i.e. any significant improvement in extended cycling will be measurable in a few cycles under these extremely aggressive conditions). Therefore, although direct comparison to retention from galvanostatic studies is impossible, comparisons herein for our 1300 samples over 10 cycles are highly meaningful. Density functional

theory was used to study the diffusion path of Li in the undoped LCP (Fig. 1d) and yields an energy barrier of 0.30 eV as shown in Figure S2. It should also be noted that these aggressive cycling conditions contribute to the overpotential which can be seen to be large in Fig. 1c.

Having benchmarked the undoped material with our high-throughput methods, a single dopant screening was performed at a 10% substitution for Co, denoted as $Li_yCo_{0.9}M_{0.1}PO_4$ yielding the samples shown in Fig. 1e. In total, 46 elements were attempted, covering a very large portion of the periodic table as shown in Figure S1. The Li content (y) self-adjusts to compensate for the oxidation state of the M dopant (excess Li evaporates during synthesis in air at or above 750 °C).[19] Detailed XRD analysis is required to determine to what extent substitution into LCP takes place. It is highly useful for us here that LCP exists as a single composition in the Li-Co-PO_4 pseudoternary phase diagram[20] such that any change in lattice parameter can be attributed to the substituent being integrated (at least partially) into the LCP structure. Multi-phase Rietveld refinement was utilized to obtain phase percentages based on known CIF files in the ICSD database and extract lattice parameters. A full list of the results for 750 and 850 °C are shown in Tables S1-S2 with a complete list of secondary phases, and Figs. 3 and S3. The phase fractions were then used with their cobalt and dopant contents to calculate what fraction of the dopant was present in the LCP phase. This is considered to be precise except for the patterns that had peaks that could not be indexed (these are marked by a * in Fig. 3 and S3). We find that 57 % of dopants were integrated in LCP (> 5 % doping) at 750 °C, while 67 % were integrated at 850 °C. This large set of data therefore leads to some important conclusions: (i) the solubility of dopants is generally quite high, (ii) many dopants show better solubility at 850 °C than 750 °C (though a few, like Ti, decreased at the higher temperature), (iii) a few dopants like Al show quite low solubility. As will be discussed below, a number of the samples of highest interest for improved electrochemistry

also show high doping (e.g. In, Re, Zn). It should also be noted that the unidentified phase in the In-substituted sample is quite small and is not seen when the In content is < 10 % as discussed below.

Combinatorial cyclic voltammetry was performed on the single-dopant samples as shown in Figs. 4, S4-S5. Average discharge voltage, average overpotential (charge – discharge), specific capacity on first discharge, reversible capacity on the first cycle, and capacity retention after 10 cycles are all extracted from the CVs and plotted in Figs. 4 and S6. Compared to the undoped samples with capacities near 100 mAh/g and capacity retention around 45 %, many of the substituted samples show a dramatically improved capacity, despite the fact that the theoretical capacity has dropped from 167 mAh/g to 150 mAh/g assuming the substituent is electrochemically inactive. There are definite trends in the properties evolution in Fig. 4, such as the inverted volcano in the capacity in the 4th period where In and Y at either end show higher capacities with a minima in the middle of the period (Mo, Rh). Ultimately, while 3d metals, which have been well studied as dopants in LCP, do show some improvement over the undoped, it is of high interest that we find greatly improved performance for a number of substituents that have generally been ignored including Ga, In, Re, and Au. In also shows an increased discharge voltage (highest average discharge voltage among dopants), a low overpotential, and an increased reversibility; all despite the fact that In^{3+} is electrochemically inactive.

To better understand the role of indium, samples with various In content were prepared ranging from 0.1 % to 100 %, as shown in Figure 5. The XRD patterns show clear phase co-existence above 10 % (quantified in Figure S7), but 5 % substitution and below yielded single phase LCP, with the lattice parameters showing significant changes up to 5 % as shown in Fig. 5b (even 0.1 % expands *a* while contracting *b* and *c*). Importantly, Figure 5d clearly shows that the benefits of

indium are seen over a wide range of doping levels, with the theoretical capacities being fully achieved at both 1 and 5 %, and the highest capacity of 161 mAh/g at 1 % In substitution being particularly competitive. Figure S7 shows the corresponding average discharge potentials, which generally increase with In content, in contrast to previous computational predictions[6] such that the source of the increase seen here will be discussed further below. It should be noted that other dopants were also studied at this stage of the current study but none performed as well at lower doping levels as at 10 %, except In (e.g. Re showed a diminished capacity of 110 mAh/g at 5%). Thus, our focus here will be on In-doping. Despite the above success, In-substituted samples consistently show a capacity retention of approximately 60 % over 10 cycles, regardless of In content. The sources of these effects were explored both using DFT calculations and conductivity measurements. Figures 5e and S2c,d show the result for the energy barrier from DFT for Li diffusion in a 12.5 % In substituted material, with details provided in **SI notes 1**. This resulted in 4 distinct activation energies, with 3 being smaller than in pure LCP (0.23 – 0.287 eV, vs 0.30 eV in pure LCP). This implies that In only lowers the barrier to Li diffusion near itself and that the 12.5% substitution used in the calculation is insufficient to create an entire diffusion path with lowered barriers. We therefore expect little to no improvement in the ionic diffusivity with In substitution, with the primary benefit being the creation of Li vacancies throughout the channels. Furthermore, the band structure shows no significant changes compared to the undoped such that we expect In-substituted LCP to continue to be electronically insulating (by contrast, the Mo-doped band structure shows defect bands that reduce the band gap as discussed in **SI notes 2**). The results for the ionic conductivity of the non-carbon coated LCP samples (Table I based on data in Fig. S8) did show a moderate improvement of about 50 %, consistent with the fact that the largest barrier to Li diffusion remains 0.30 eV in the DFT calculations such that large gains are not made.

Surprisingly though, the electronic conductivity of the carbon-coated samples significantly increased in the indium-substituted samples (by a factor of nearly 5 in the 10% sample, and a factor of 3 in the 1%). Given that the improved conductivities between 0.1 to 1% substitution correlate with the improved capacities in Fig. 5c, this strongly suggests that the primary benefit of indium is to improve the electronic conductivity of the carbon coated materials (the electronic conductivities in the uncoated materials do not improve significantly). Thus, we find that indium substitution slightly improves the ionic conductivity within the LCP particles and dramatically increases the electronic conductivity of the carbon-coated materials, giving rise to near theoretical capacities in the 1 – 5 % indium-substitution ranges and the reduced overpotential in Figs. 4a,e as compared to the undoped.

Next, the important limitation of poor extended cycling must now be addressed. This motivates the utilization of co-doping in this material: utilize one element to increase energy density (e.g. In) and a second to improve the extended cycling. Systematic co-doping was therefore performed on 5% In, 5% M samples made at 850 °C (the higher temperature being selected due to overall improvement in electrochemistry in the single-substituted samples and higher level of doping obtained based on XRD). The lattice parameter shifts for the In/M co-substituted LCP phases based on XRD data are shown in Fig. S9, and the most common change seen is to expand the *a* lattice and contract *b, c* (the exact opposite of what was found in adding 5% In to the undoped as discussed above). While in the single dopant situation, it was possible to extract the fraction of dopant in the LCP structure, here it is not. There are too many possible compositions of the secondary phases which could contain either dopant or both. The CVs (Fig. S10) show wide variations as was the case in the single-substitution case, and extracted battery performance metrics are shown in Fig. 6. In the co-substitution case, there is no dramatic improvement in capacities, however there are

samples with greatly improved capacity retention. A number of samples retained more than 90 %, and Mo/In co-doped in fact retained 100 % (although with a more moderate capacity of 100 mAh/g). Figures 2 and S11 show SEM images of In/Mo co-doped samples, with the morphology being dramatically impacted by the presence of Mo with massive 10-30 micron spherical particles making up the vast majority of the sample. Considering the size of particles, the capacities of 100 mAh/g are a testament to the improved transport properties in the doped samples (undoped particles of about 5-10 microns obtained a capacity of 5 mAh/g in ref.[21]). Given the large particles in the Mo/In co-doped samples, there is less surface area available for electrolyte oxidation in this sample as compared to the others shown in Fig. 2 where a far greater number of smaller particles make up the electrode. The reduced surface area results in less electrolyte oxidation and this certainly contributes to the improved extended cycling obtained for Mo/In co-doping.

DFT calculations (detailed in **SI notes 3**) were also performed for a set of dopants to determine the formation energy for Li/Co antisite defects to better understand why some dopants (e.g. Nb) improved the capacity retention, while others like Al did not. Such antisite defects are commonly correlated to poor extended cycling in LCP.[22] Figure 7a shows the results for all possible Li/Co defects in the structures. The undoped and Al doped both show that some defects will form spontaneously (negative formation energy). While In-substitution results in defects requiring energy to form, the energy is small. We attribute the slight improvement in extended cycling in the In single dopant samples (60 % vs 45 % in undoped) to this change in formation energy. By contrast, other substituents such as Mo and Nb result in a dramatic increase in the formation energy. This explains why co-doping was so effective in further improving the extended cycling.

Seeing the dramatic improvement in extended cycling with co-doping, we explored more compositions of the In/Mo and In/Nb co-doped samples to see if the two key effects (improved

capacity and extended cycling) could be optimized simultaneously. The best results were found to be for In/Mo as shown in Fig. 7d,e. For very moderate substitution levels (1% of each of In and Mo), capacities as high as 150 mAh/g were obtained along with a well improved retention of 75 % (compared to 60 % in In-single dopant, or 50 % in pure LCP), again under very harsh cycling conditions (CV up to 5.3 V). By contrast, In/Nb showed a retention that was not improved over the singly In-doped samples. We also confirm that the high performance for In/Mo co-doping is maintained when cycled under galvanostatic conditions in a coin cell. Figure S18 and Table S4 show that both 1%/1% and 5%/5% co-doped samples have first discharge capacities (150 and 80 mAh/g, respectively) in good agreement with the high-throughput CV work reported above (152 and 100 mAh/g, respectively). Similarly, the extended cycling is considerably better in the 5%/5% sample as compared to the 1%/1% sample (e.g. 98% vs 89% on the second cycle, and 85% vs 70% after 5 cycles), again consistent with the HT voltammetry. Though further work is needed to develop bulk synthesis of these materials and couple them to improved electrolytes, the results clearly indicate that the optimized co-doped materials show improved performance under galvanostatic conditions as well as cyclic voltammetry.

3. Conclusions

This work was focused on improving the performance of a very challenging high voltage cathode material for Li-ion batteries: $LiCoPO_4$ with a peak potential of about 4.8 V *vs*. Li. A total of 1300 samples were studied, with 263 distinct substituted samples with numerous duplicates to ensure reproducibility (e.g. the 10% In-doped samples had 11 duplicates and yielded a low standard error of about 3 mAh/g on an average capacity of 133 mAh/g). This work clearly demonstrates the extent to which the design of advanced battery cathodes can be accelerated with the use of high-

throughput experimental screening to study the impact of composition and synthesis conditions on a wide variety of properties of importance for battery performance. Herein, certain electrochemically inactive dopants were found to dramatically improve the first cycle capacity by improving both ionic and electronic conductivity in carbon-coated materials. Co-doping was found to greatly improve the extended cycling by both preventing antisite defects and producing larger particles thereby minimizing the surface area per unit mass of cathode where electrolyte decomposition occurs at the very high potentials utilized here. The improvement from 95 mAh/g, 43 % retention in unsubstituted LCP to 150 mAh/g with 75 % retention with only 2% substitution of the cobalt with In/Mo is truly remarkable. This is especially noteworthy when one considers that all materials were cycled under the same harsh conditions of cyclic voltammetry up to 5.3 V (i.e. all samples spent 3 h above 5 V every cycle), such that improved extended cycling is truly significant. The dramatic improvement with In/Mo co-substitution was attributed to numerous factors: (i) improved Li diffusion with the addition of In, (ii) larger particles with the addition of Mo, (iii) improved electronic conductivity in the carbon-coated material with the addition of In, and (iv) suppression of Li/Co antisite defects by the addition of both In and Mo. Given the wide variety of properties manipulated through the substitutions (morphology, defect suppression, lattice distortion to enable Li diffusion, nature of C-coating changing the electronic conductivity), high-throughput experiments are not only shown to be useful but in fact are necessary to design an optimum material. This work not only produces a novel state-of-the-art material (In/Mo co-doped LCP) despite decades of previous work on LCP, but also serves as a template for how to accelerate the design of cathodes for advanced batteries using high-throughput experimentation, complemented with traditional experimental and computational methods.

4. Experimental section

Synthesis

A citrate sol-gel method was used to prepare the samples. The optimal mole ratio of total metals to citric acid was 1:1. $LiNO_3$ (2M), $Co(NO_3)_2$(2M), $(NH_4)_2HPO_4$ (2M), and citric acid (4M) solutions were prepared in deionized water. The concertation of the initial metal solutions was quantified by inductively coupled plasma–optical emission spectroscopy (ICP–OES). First, 40 µL of citric acid was pipetted into 64 (400 µL alumina) cups followed by the addition of 40 µL of cobalt nitrate, 40 µL of lithium nitrate, and lastly 40 µL of ammonium phosphate dibasic. An aluminum smokestack was placed on the cups to prevent cross-contamination during gel swelling. The bulk of the water was reduced by heating to 70 °C for 12 h yielding a viscous gel. The rest of the trapped water was removed by incremental heating starting from 100 °C to 200 °C under vacuum, producing brown color powder that was ground before further heat treatment in air. These powder samples were heated to 750 °C or 850 °C for 4 h at a ramp/cool rate of 5 °/min. The violet colored powder formed was ground and placed on top of an alumina plate in clamps (~10 mg) and then wetted with 12 µL of 104 g/L citric acid corresponding to 13%wt citric acid content (10 %wt carbon). The wetted clamps were mixed by a pin forming a slurry. These slurries were transferred to a tube furnace and heated to 650 °C for 30 min at a ramp rate of 2 °C/min under an Ar:H_2 (95:5) atmosphere. After the coating step, the black/gray samples were ground for the structural and subsequently electrochemical analysis.

Characterization

The carbon-coated samples were transferred into a high throughput XRD holder. Their diffraction patterns were collected in transmission mode using PANalytical diffractometer equipped with a Mo anode X-ray source (60 kV, 40 mA) and GaliPIX3D area detector. The phases present were identified using the matching tool in HighScore Plus by searching against open crystal and ICSD

databases. Once all the phases were identified, Rietveld refinement was performed to determine the content of each phase and their lattice parameters. For convenience, the patterns shown in this paper are K-alpha stripped and wavelength converted from Mo to Cu. The morphology of the samples was characterized by scanning electron microscopy (SEM) using a Hitachi SU3500 at 30 keV. The XPS measurement was done using a Thermo Scientific K-Alpha spectrometer equipped with Al Kα micro-focused monochromator. The XPS measurement was done at a pressure of <~ 10^{-7} mbar with an X-ray spot size of 200 μm. The survey and high-resolution spectra were collected with a pass energy of 200 eV and 50 eV, respectively. All binding energies were calibrated using the C 1s peak (284.8 eV).

High-throughput cyclic voltammetry

The high-throughput electrochemical analysis was performed by the lab-build high-throughput cyclic voltammetry system, which was designed by the Dahn lab[23] and adapted for use with cathode powders by the McCalla lab[24–26]. In detail, the custom-designed printed circuit board (PCB) covered with aluminum pads has the capability to test 64 channels simultaneously, as illustrated in Figs. S12. To prepare the electrodes, about 8 mg of each active material (AM) were weighed out and mixed with a slurry containing 80 μL N-methyl-2-pyrrolidone (NMP) (Alfa Aesar) containing 0.45 mg polyvinylidene fluoride (PVDF) (Kynar 1100), and 1.04 mg carbon black (TIMCAL). After mixing with a stirring rod for 15 min, the cathode was prepared by drop-casting 3 μL of the above-mentioned slurry onto the appropriate pad of the PCB. The electrodes were then dried at 80 °C for 12 h. The resulting electrode formulation is 84 wt % AM, 11 wt % carbon black, and 5 wt % PVDF, and the AM loading was typically 2.4 mg/cm^2 with a thickness of about 100 μm (minor variations were seen due to the shape of the electrode after drying, see Fig. S12 as an example). The combinatorial cell was then assembled in an argon-filled glovebox

with the electrolyte (1M LiPF6 in 1:1 EC: DMC, SoulBrain MI) soaking two Whatman microfiber separators, and Li metal as the counter electrode. The cell is shown schematically in Fig. S13. The CVs were performed with the voltage range from 3.0 V to 5.3 V vs. Li/Li^+ at a scan rate of 0.2 V h^{-1}.

Galvanostatic cycling

In order to ensure that the high performance of the In/Mo co-doped samples is maintained in galvanostatic cycling conditions, a slurry was made from 30 mg of LCP (multiple HT samples were combined to achieve this) with a formulation of 85 % AM, 7.5 % carbon black and 7.5 % PVDF. Electrodes with a mass loading of 2.5 mg/cm^2 were prepared using a doctor blade and then assembled into LIR2032 type coin cells (MTI Corp.) with the same electrolyte as in the HT voltammetry measurements. Galvanostatic cycling was performed at 10 mA/g in the range 3.0 – 5.0 V on a Biologic potentiostat.

Conductivity measurements

The electronic and ionic conductivities were measured by cold pressing 30 mg samples using a 3 mm pressing die and coating two gold blocking electrodes as contacts. The total electrical conductivity was determined by electrochemical impedance spectroscopy (EIS) using Biologic SP150. The EIS spectra were collected by scanning from 1 MHz to 100 mHz with an AC amplitude of 100 mV. The EIS Nyquist plots were fitted to the proper equivalent circuit using EC-lab. The electronic conductivity was determined by applying 1.5 V DC polarization for 15 min while measuring the current decay. From the steady-state current, the electronic contribution was calculated.

Density functional theory

First-principles calculations were performed with the Perdew–Burke–Ernzerhof (PBE) exchange-correlation functional using the spin-polarized GGA[27]. The projector-augmented wave pseudopotentials were used as implemented in the Vienna Ab initio Simulation Package (VASP)[28]. A Hubbard-type U parameter (GGA + U)[29] was added to correct the on-site Coulomb interactions, with U[Co] = 5.7 eV[30], U[In] = 7.0 eV[31], U[Mo] = 3.5 eV[32] and U[Nb] = 3.02 eV[33]. The supercell of LCP was 2a x 2b x 1c, comprising 112 atoms ($Li_{16}Co_{16}P_{16}O_{64}$). The magnetic ordering preference of LCP was calculated to demonstrate the intrinsic antiferromagnetism in LCP.[34] The activation barriers of Li migration were calculated using the CI-NEB method[35,36]. All the lattice parameters were fixed, but all the atomic positions were relaxed within the supercell during the CI-NEB calculations. To avoid the charge ordering problem on transition metals within GGA + U, the elastic band was calculated without U correction[30].

Supplemental Information

Supporting information associated with this paper is available online.

Acknowledgments

This work was primarily funded by the Samsung Advanced Institute of Technology and additionally funded by NSERC under the auspices of a discovery grant and the Canadian Foundation for Innovation.

References

1. Zhang, M., Garcia-Araez, N. & Hector, A. L. Understanding and development of olivine LiCoPO4 cathode materials for lithium-ion batteries. *J. Mater. Chem. A* **6**, 14483–14517 (2018).

2. Fan, X. & Wang, C. High-voltage liquid electrolytes for Li batteries: progress and perspectives. *Chemical Society Reviews* **50**, 10486–10566 (2021).
3. Li, J. & Ma, Z.-F. Past and Present of LiFePO4: From Fundamental Research to Industrial Applications. *Chem* **5**, 3–6 (2019).
4. Ludwig, J. *et al.* Morphology-controlled microwave-assisted solvothermal synthesis of high-performance LiCoPO4 as a high-voltage cathode material for Li-ion batteries. *Journal of Power Sources* **342**, 214–223 (2017).
5. Li, H. *et al.* Improved electrochemical performance of 5V LiCoPO4 cathode materials via yttrium doping. *Solid State Ionics* **255**, 84–88 (2014).
6. Zhi-Ping, L., Yu-Jun, Z. & Yan-Ming, Z. Li- Site and Metal-Site Ion Doping in Phosphate-Olivine LiCoPO4 by First-Principles Calculation. *Chinese Phys. Lett.* **26**, 038202 (2009).
7. Cherkashinin, G. *et al.* Energy Level Alignment at the Cobalt Phosphate/Electrolyte Interface: Intrinsic Stability vs Interfacial Chemical Reactions in 5 V Lithium Ion Batteries. *ACS Appl. Mater. Interfaces* **14**, 543–556 (2022).
8. Wolfenstine, J. Electrical conductivity of doped LiCoPO4. *Journal of Power Sources* **158**, 1431–1435 (2006).
9. Allen, J. L. *et al.* Cr and Si Substituted-LiCo0.9Fe0.1PO4: Structure, full and half Li-ion cell performance. *Journal of Power Sources* **327**, 229–234 (2016).
10. Wang, Y. *et al.* Cr-substituted LiCoPO4 core with a conductive carbon layer towards high-voltage lithium-ion batteries. *Journal of Solid State Chemistry* **258**, 32–41 (2018).
11. Li, H. *et al.* Improved electrochemical performance of 5V LiCoPO4 cathode materials via yttrium doping. *Solid State Ionics* **255**, 84–88 (2014).

12. Allen, J. L. *et al.* Transport properties of LiCoPO4 and Fe-substituted LiCoPO4. *Journal of Power Sources* **254**, 204–208 (2014).
13. Kreder, K. J. & Manthiram, A. Vanadium-Substituted LiCoPO4 Core with a Monolithic LiFePO4 Shell for High-Voltage Lithium-Ion Batteries. *ACS Energy Lett.* **2**, 64–69 (2017).
14. Fang, L., Zhang, H., Zhang, Y., Liu, L. & Wang, Y. Design and synthesis of two-dimensional porous Fe-doped LiCoPO4 nano-plates as improved cathode for lithium ion batteries. *Journal of Power Sources* **312**, 101–108 (2016).
15. Kishore, M. V. V. M. S. & Varadaraju, U. V. Influence of isovalent ion substitution on the electrochemical performance of LiCoPO4. *Materials Research Bulletin* **40**, 1705–1712 (2005).
16. Dimesso, L., Spanheimer, C. & Jaegermann, W. Influence of isovalent ions (Ca and Mg) on the properties of LiCo0.9M0.1PO4 powders. *Journal of Power Sources* **243**, 668–675 (2013).
17. Karthickprabhu, S., Hirankumar, G., Maheswaran, A., Daries Bella, R. S. & Sanjeeviraja, C. Structural and electrical studies on Zn2+ doped LiCoPO4. *Journal of Electrostatics* **72**, 181–186 (2014).
18. Shanmukaraj, D. & Murugan, R. Synthesis and characterization of LiNiyCo1−yPO4 (y=0–1) cathode materials for lithium secondary batteries. *Ionics* **10**, 88–92 (2004).
19. McCalla, E., Carey, G. H. & Dahn, J. R. Lithium loss mechanisms during synthesis of layered LixNi2−xO2 for lithium ion batteries. *Solid State Ionics* **219**, 11–19 (2012).
20. Lin, X. *et al.* Phase relation of Li2O–CoO–P2O5 ternary system and electrochemical behaviors of Co-base polyphosphates within this system. *Journal of Alloys and Compounds* **646**, 727–733 (2015).

21. Wu, B. *et al.* Controlled solvothermal synthesis and electrochemical performance of LiCoPO4 submicron single crystals as a cathode material for lithium ion batteries. *Journal of Power Sources* **304**, 181–188 (2016).
22. Wu, X. *et al.* Investigation of the Li–Co antisite exchange in Fe-substituted LiCoPO4 cathode for high-voltage lithium ion batteries. *Energy Storage Materials* **22**, 138–146 (2019).
23. Fleischauer, M. D. *et al.* Design and Testing of a 64-Channel Combinatorial Electrochemical Cell. *J. Electrochem. Soc.* **150**, A1465 (2003).
24. Potts, K. P., Grignon, E. & McCalla, E. Accelerated Screening of High-Energy Lithium-Ion Battery Cathodes. *ACS Appl. Energy Mater.* **2**, 8388–8393 (2019).
25. Adhikari, T. *et al.* Development of High-Throughput Methods for Sodium-Ion Battery Cathodes. *ACS Comb. Sci.* **22**, 311–318 (2020).
26. Jia, S., Counsell, J., Adamič, M., Jonderian, A. & McCalla, E. High-throughput design of Na–Fe–Mn–O cathodes for Na-ion batteries. *Journal of Materials Chemistry A* **10**, 251–265 (2022).
27. Perdew, J. P., Burke, K. & Ernzerhof, M. Generalized Gradient Approximation Made Simple. *Phys. Rev. Lett.* **77**, 3865–3868 (1996).
28. Kresse, G. & Furthmüller, J. Efficient iterative schemes for ab initio total-energy calculations using a plane-wave basis set. *Phys. Rev. B* **54**, 11169–11186 (1996).
29. Dudarev, S. L., Botton, G. A., Savrasov, S. Y., Humphreys, C. J. & Sutton, A. P. Electron-energy-loss spectra and the structural stability of nickel oxide: An LSDA+U study. *Phys. Rev. B* **57**, 1505–1509 (1998).

30. Ping Ong, S. *et al.* Voltage, stability and diffusion barrier differences between sodium-ion and lithium-ion intercalation materials. *Energy & Environmental Science* **4**, 3680–3688 (2011).
31. Ágoston, P., Erhart, P., Klein, A. & Albe, K. Geometry, electronic structure and thermodynamic stability of intrinsic point defects in indium oxide. *J. Phys.: Condens. Matter* **21**, 455801 (2009).
32. Rellán-Piñeiro, M. & López, N. One Oxygen Vacancy, Two Charge States: Characterization of Reduced α-MoO3(010) through Theoretical Methods. *J. Phys. Chem. Lett.* **9**, 2568–2573 (2018).
33. Pasquier, D. & Yazyev, O. V. Charge density wave phase, Mottness, and ferromagnetism in monolayer 1 T− NbSe 2. *Phys. Rev. B* **98**, 045114 (2018).
34. Gnewuch, S. & Rodriguez, E. E. Distinguishing the Intrinsic Antiferromagnetism in Polycrystalline LiCoPO4 and LiMnPO4 Olivines. *Inorg. Chem.* **59**, 5883–5895 (2020).
35. Henkelman, G. & Jónsson, H. Improved tangent estimate in the nudged elastic band method for finding minimum energy paths and saddle points. *J. Chem. Phys.* **113**, 9978–9985 (2000).
36. Henkelman, G., Uberuaga, B. P. & Jónsson, H. A climbing image nudged elastic band method for finding saddle points and minimum energy paths. *J. Chem. Phys.* **113**, 9901–9904 (2000).
37. Jonderian, A. *et al.* Suite of High-Throughput Experiments for Screening Solid Electrolytes for Li Batteries. *J. Electrochem. Soc.* **169**, 050504 (2022).

Tables:

Table 1. Ionic and electronic conductivities measured on cold pressed pellets of various LCP samples. The electronic conductivity was determined using DC measurements in a Au/LCP/Au configuration as per ref.[37]. The ionic conductivities were extracted by fitting the EIS spectra with an equivalent circuit for a mixed conductor (the second conductor corresponding to the electronic conductivity, the extracted value from EIS matched that from DC measurements as expected). Typical patterns of each are shown in Figure S8. Carbon coated samples are denoted with @C.

Sample	σ_i (S cm^{-1})	σ_e (S cm^{-1})
$LiCoPO_4$@C	6.9×10^{-7}	5.4×10^{-7}
$Li_{0.999}Co_{0.999}In_{0.001}PO_4$@C	5.2×10^{-7}	7.1×10^{-7}
$Li_{0.99}Co_{0.99}In_{0.01}PO_4$@C	4.1×10^{-7}	1.6×10^{-6}
$Li_{0.975}Co_{0.975}In_{0.025}PO_4$@C	8.1×10^{-7}	1.3×10^{-6}
$Li_{0.95}Co_{0.95}In_{0.05}PO_4$@C	7.5×10^{-7}	2.2×10^{-6}
$Li_{0.9}Co_{0.9}In_{0.1}PO_4$@C	7.7×10^{-7}	2.5×10^{-6}
$Li_{0.85}Co_{0.85}In_{0.15}PO_4$@C	7.2×10^{-7}	1.8×10^{-6}
$LiCoPO_4$	1.2×10^{-7}	4.2×10^{-8}
$Li_{0.9}Co_{0.9}In_{0.1}PO_4$	1.8×10^{-7}	5.5×10^{-8}

Figures

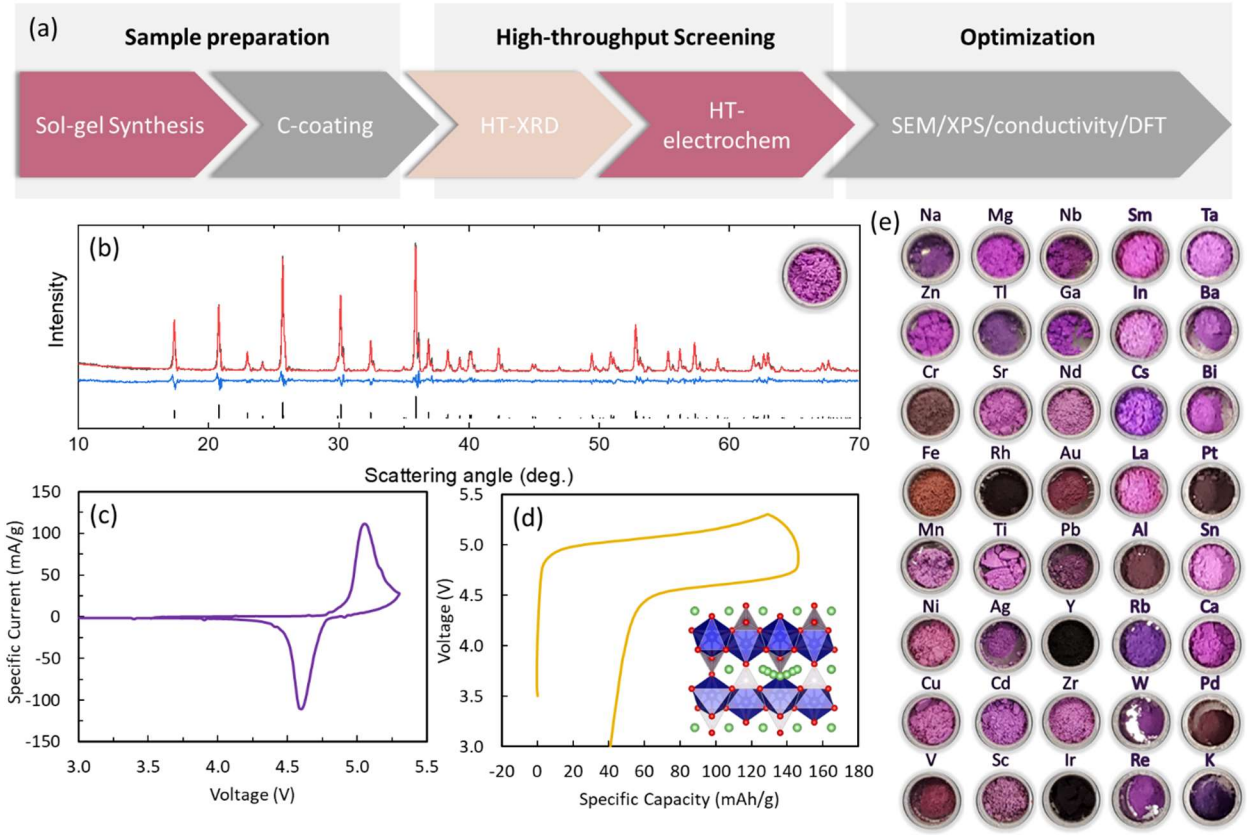

Figure 1. (a) Workflow for the current study where high-throughput (HT) synthesis/characterization is used to screen cathode materials, followed by traditional experiments/computations to motivate further HT tests. X-ray diffraction (b) and electrochemistry (c,d) of the undoped sample made at 850 °C show limited capacity and high overpotentials, while the Li diffusion path in the undoped is shown in (d). (e) Pictures of the $Li_yCo_{0.9}M_{0.1}PO_4$ samples after heating in air to 750 °C (prior to carbon coating).

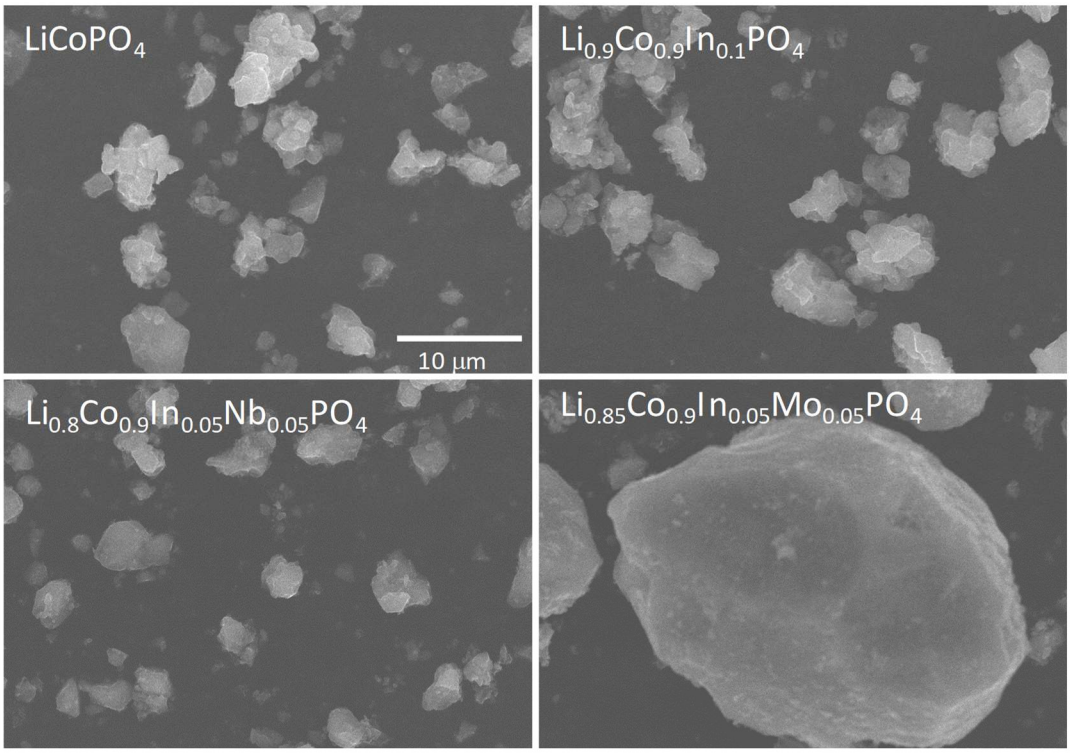

Figure 2. SEM images of unsubstituted LCP along with 10% In-doped, as well as In/Mo and In/Nb co-doped samples. In all cases the images are representative. The scale bar applies to all four SEM images.

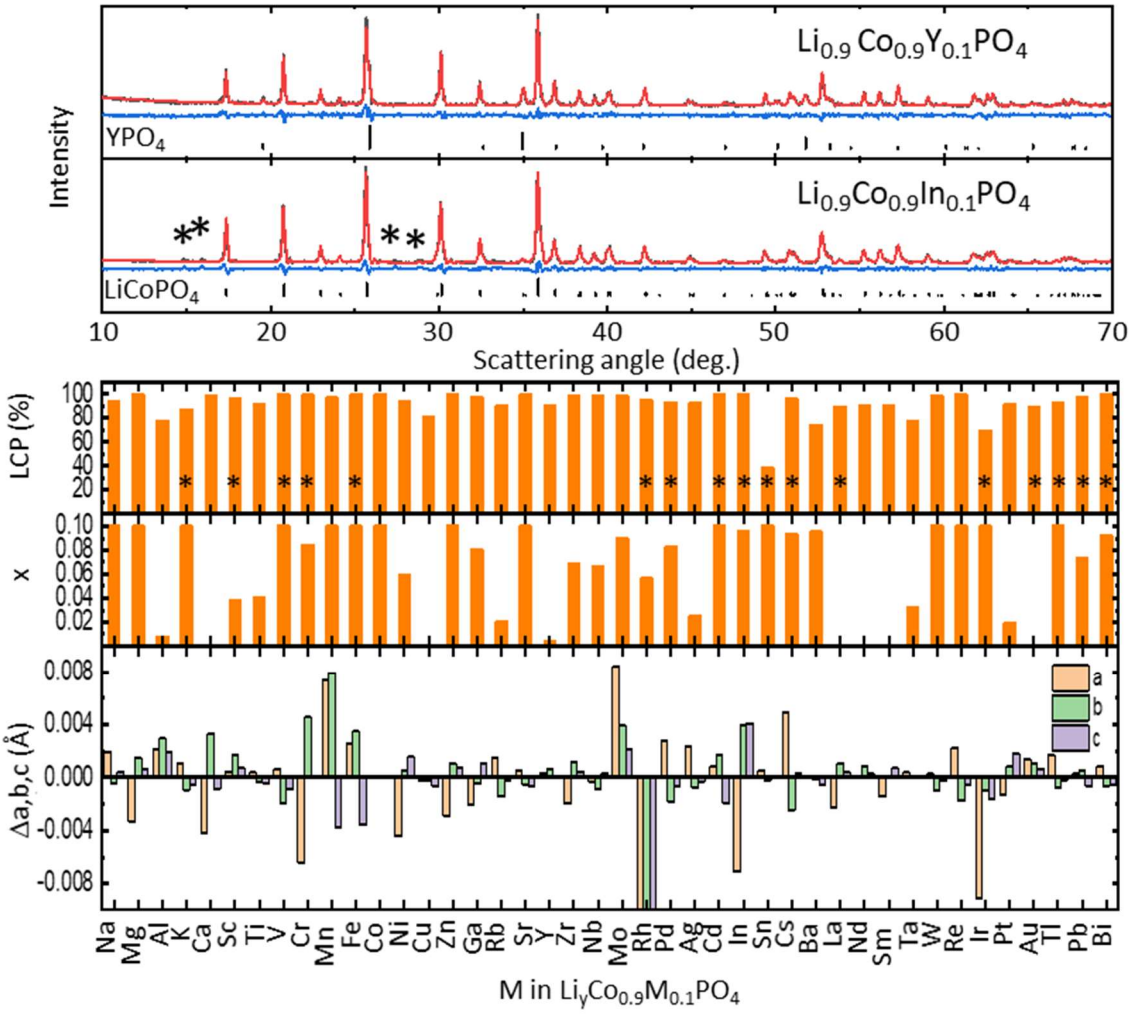

Figure 3. XRD results for single dopant samples heated at 850 °C and carbon coated. Top: two representative XRD patterns along with the fits in red and the difference plots in blue. The * indicates small peaks corresponding to the unidentified phase in the In-doped sample. Lower: extracted values for molar phase % of the olivine LCP phase, * indicates the presence of an unidentified phase, x (the calculated x-value in $Li_yCo_{1-x}M_xPO_4$ as detailed in the SI), and the shift in lattice parameters with respect to the undoped samples (standard deviations in undoped duplicates were less than 0.0002 Å).

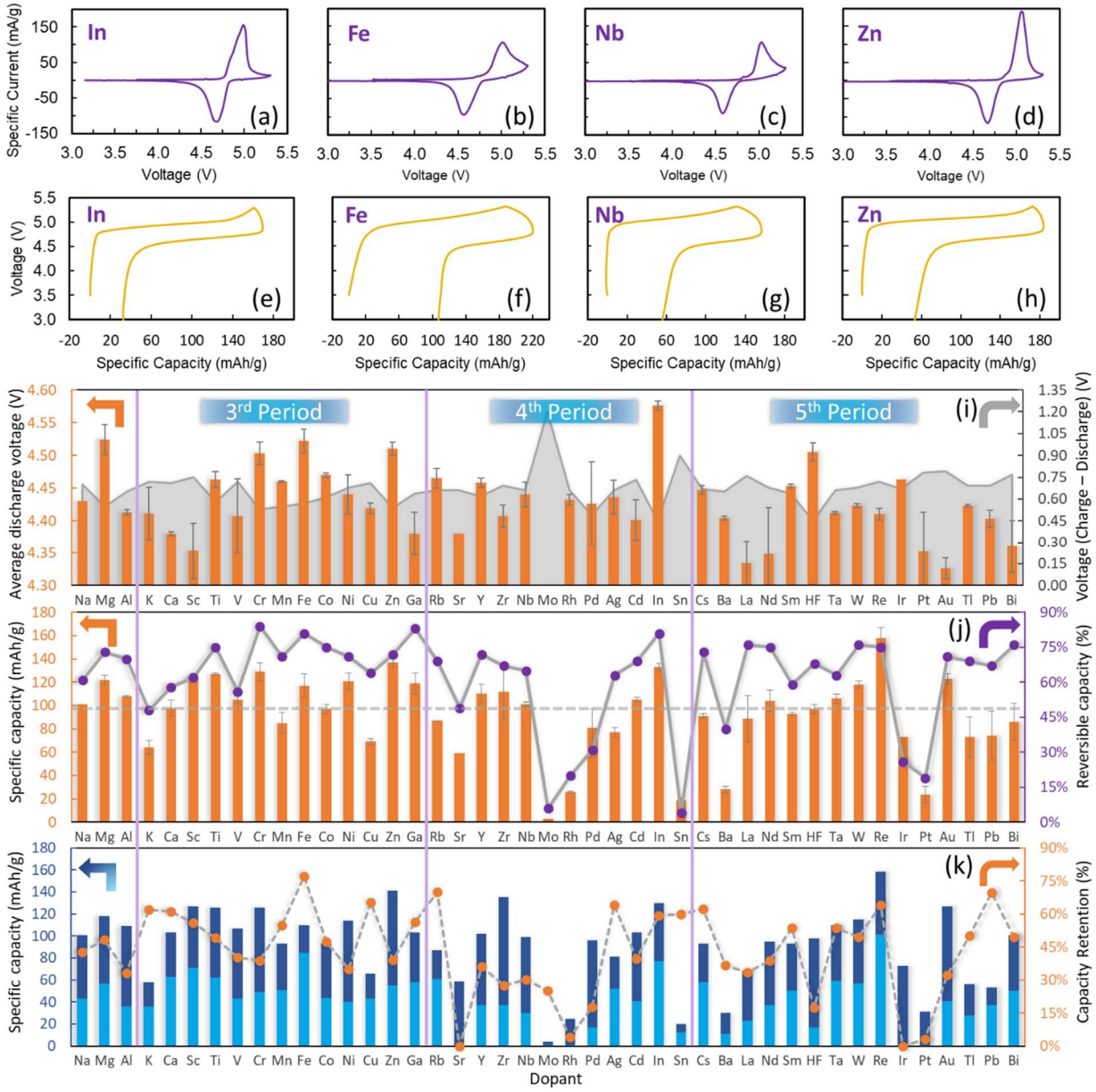

Figure 4. Results of the high-throughput electrochemical testing on the $Li_yCo_{0.9}M_{0.1}PO_4$ samples prepared at 850 °C in air prior to carbon coating. Representative CVs (a-d) and corresponding voltage curves (e-h) are shown. The properties extracted for the first cycle are shown in (i,j) while (k) shows the retention after 10 cycles. The grey dashed line in (j) indicates the discharge capacity of the undoped sample as a reference. While a number of samples show significantly improved capacities, the retention continues to be poor.

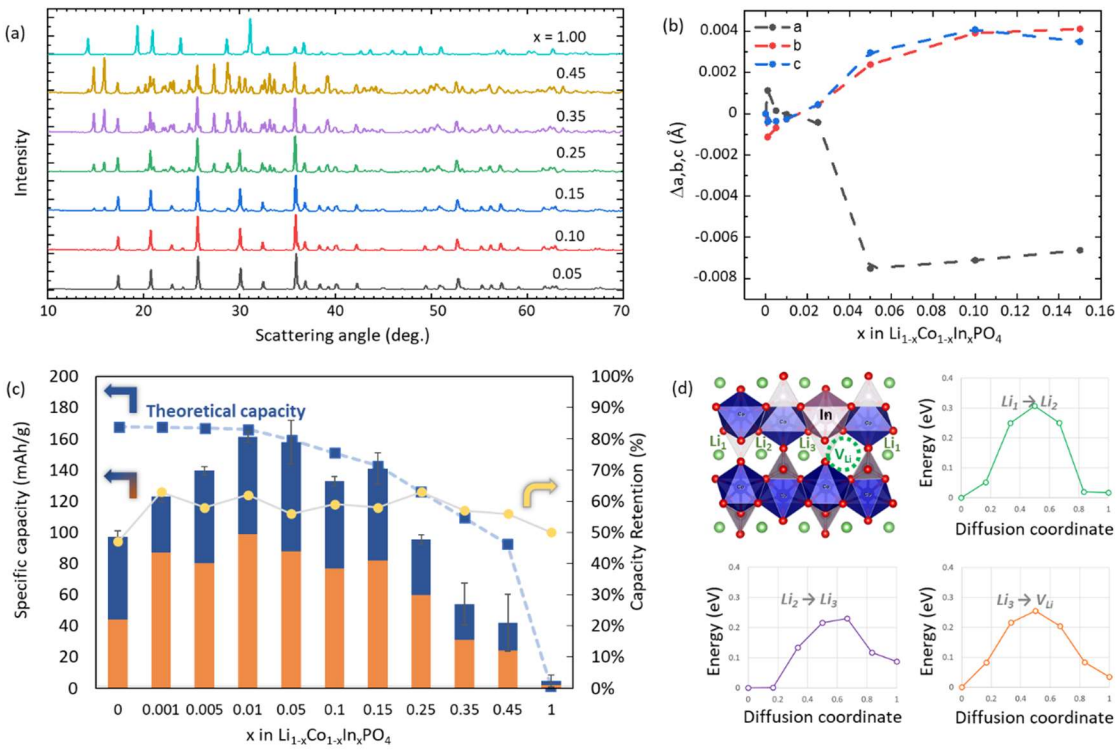

Figure 5. Results for In-doped samples with varying In content. The XRD results in (a) yield the shifts in lattice parameters shown in (b). Phase pure materials are obtained below 10% In substitution. The resulting electrochemical data is shown in (c) along with the theoretical capacities assuming electrochemically inactive In. (d) Results of DFT calculations for the energy barriers of Li diffusion along the paths indicated in the structure, the position of the In atom and Li vacancy are also shown.

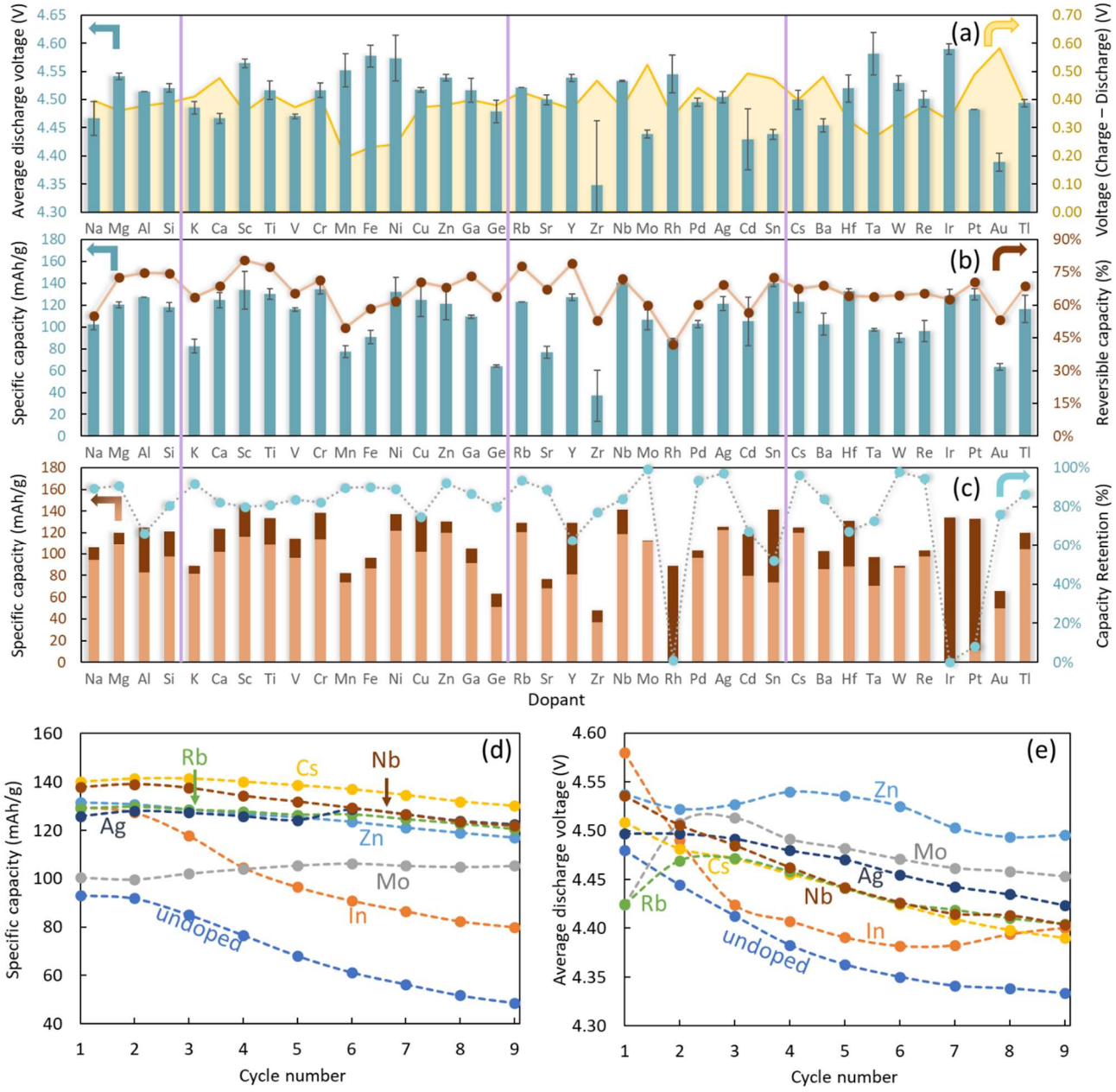

Figure 6. Battery properties extracted for the $Li_yCo_{0.9}In_{0.05}M_{0.05}PO_4$ samples. The first cycle average voltages and capacities are shown in (a), (b), respectively. (c) shows capacity retention after 9 cycles, while (d-e) show the capacities and average voltages vs. cycle number for a selection of samples with a particularly high capacity retention.

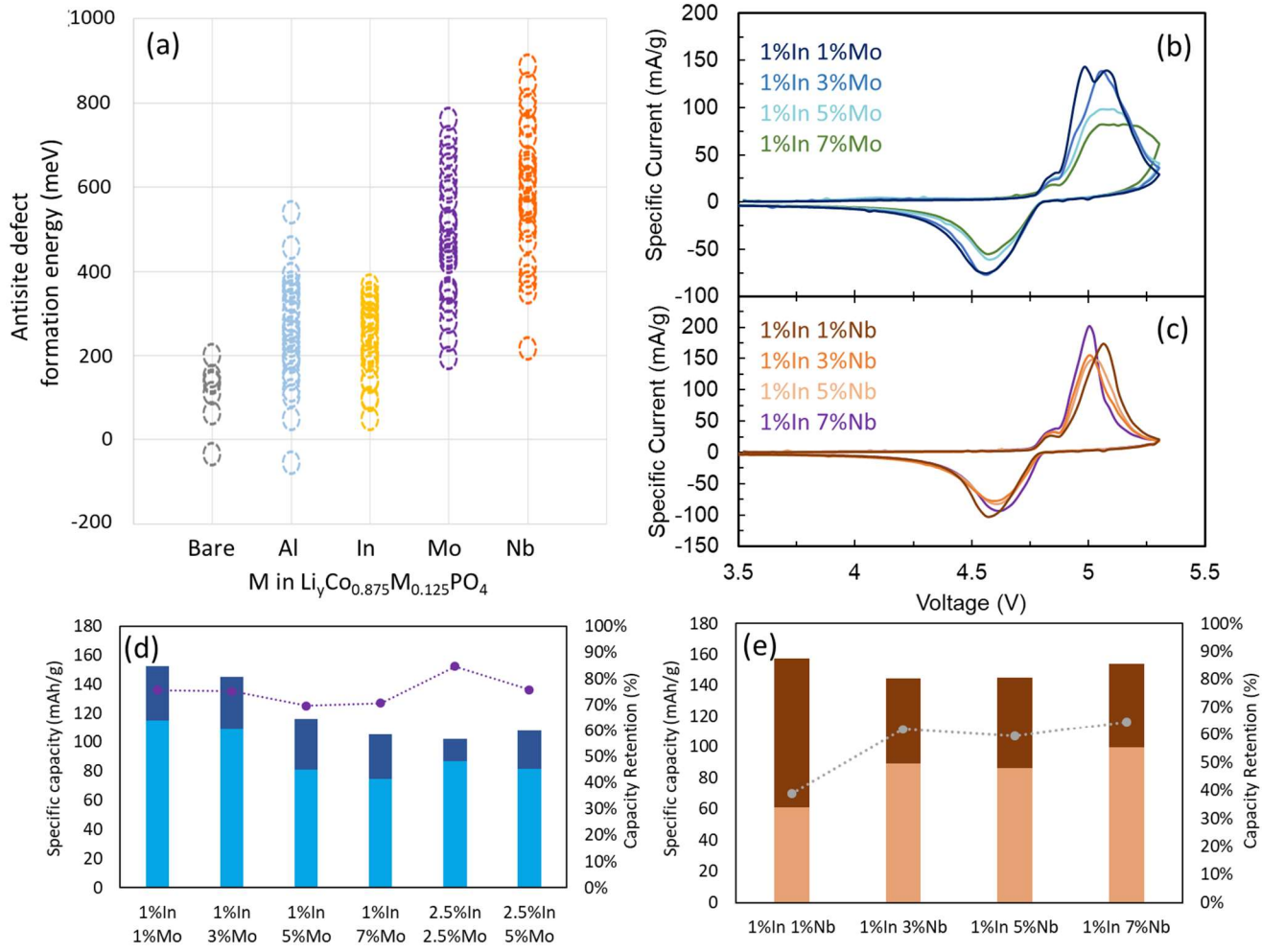

Figure 7. Results of optimization of co-doping with indium. Results of DFT calculations (a) show which dopants are most effective in suppressing Li/Co antisite defects. The first cycles of CVs for various co-doping with either Mo (b) or Nb (c) are shown, while (d,e) show the corresponding capacity retentions after 10 cycles.

Table of contents graphic: